Interference effect in high-order harmonic generation from degenerate current-carrying orbitals of polyatomic molecules

Dian Wang,[1] Xiaosong Zhu,[1,*] Hua Yuan,[1] Pengfei Lan,[1] and Peixiang Lu[1,2,†]

[1]*School of Physics and Wuhan National Laboratory for Optoelectronics, Huazhong University of Science and Technology, Wuhan 430074, China*

[2]*Hubei Key Laboratory of Optical Information and Pattern Recognition, Wuhan Institute of Technology, Wuhan 430205, China*

(Received 9 August 2019; accepted 23 January 2020; published 12 February 2020)

When the molecules with degenerate current-carrying orbitals are exposed to the bichromatic counterrotating circularly polarized (BCCP) laser fields, the destructive interference between high harmonics from these orbitals results in a strong suppression of harmonic emission with the selected helicity. As a result, there are large intensity differences between the high harmonics with opposite helicities in a wide spectral range. This interference effect is related to the noncylindrical symmetry of the molecular current-carrying orbitals and therefore depends on the relative orientation between the molecule and the driving laser fields. Furthermore, our results show that this interference can be controlled by adjusting the relative intensity ratio of the BCCP field. Finally, we show that highly elliptically polarized attosecond pulses can be generated by using this interference and their ellipticities can be tuned by controlling the molecular orientation.

DOI: 10.1103/PhysRevA.101.023406

I. INTRODUCTION

High harmonic generation (HHG) can produce attosecond bursts of extreme ultraviolet (EUV) and soft x-ray light with tabletop-scale lasers [1–4]. For a long time, high harmonics were limited to linear polarization [1,5,6], which was generally accepted as a fundamental feature of HHG due to its recollision mechanism [7,8]. On the other hand, circularly polarized radiation in EUV and soft x-ray spectral regions is of importance in applications, such as studying ultrafast chiral-specific dynamics in molecules [9,10], magnetic circular dichroism spectroscopy [11–13], the direct measurement of Berry's phase, and reconstruction of band structure in solids [14,15]. Therefore, the quest for schemes enabling the generation of circularly polarized high harmonics has attracted considerable attention.

In the past few years, several schemes were proposed to produce high harmonics with large ellipticity and high efficiency. Several works reported that the elliptically polarized high harmonics can be obtained in prealigned molecules driven by linearly polarized pulses [16–18]. However, the measured ellipticity is limited in this scheme. Recent works have demonstrated the bright circularly polarized high harmonics can be obtained through the bichromatic counterrotating circularly polarized (BCCP) fields [12,13,19–25]. However, in these works, HHG suffers from polarization degradation and eventual photon energy limits due to the spectral overlap of oppositely polarized adjacent harmonic orders, which is not favorable to synthesize highly elliptically polarized ultrafast pulses. In addition, the scheme of noncollinear counter-rotating driver pulses with the same wavelength is also proposed [11,26,27], but HHG yields in this scheme are hampered by a finite interaction length [28]. More recently, generation of circularly polarized EUV HHG has been predicted in solids [29–31]. However, HHG with highly elliptical polarization in solid targets is limited to the bandwidth nearby resonance. In the schemes with gas targets, only atoms and linear molecules (like N_2, O_2) are used as targets. Polyatomic molecules have more complex structures, which could provide more degrees of freedom for the control of HHG.

If an electron state ψ has nonzero orbital angular momentum L_z, this state possesses nonzero electronic current densities [25,32,33] calculated by $\mathbf{j} = \frac{i}{2}(\psi\nabla\psi^* - \psi^*\nabla\psi)$. Thus this state has the stationary electronic ring current around the axis of symmetry (z axis) and is called the current-carrying state. Current-carrying states have recently garnered much attention [25,32,34–39]. Atoms with p orbitals, such as Ne, have degenerated current-carrying orbitals $p_\pm$ with magnetic quantum number $m = \pm 1$, respectively. The direction of the electronic ring current of these orbitals is determined by the sign of the magnetic quantum number. Furthermore, due to the spherical symmetry of atoms, the atomic ring current is toroidal. It has been shown that these two orbitals have distinct responses to the circularly polarized field because of their opposite orbital angular momentum, i.e., the opposite direction of the ring currents [34,36–38]. Molecules with high symmetries, such as NO [32], allene, benzene [40], and Mg-porphyrin [33], also have the degenerate current-carrying states. Molecular current-carrying states can be used to produce spin-polarized photoelectrons [32] and elliptically polarized harmonics [40]. These molecular ring currents may be no longer toroidal because these molecules may not possess the cylindrical symmetry around z axis [33]. Therefore,

*zhuxiaosong@hust.edu.cn
†lupeixiang@hust.edu.cn

current-carrying orbitals of polyatomic molecules could provide more degree of freedom and involve richer physics than the current-carrying orbitals of atoms.

It has been shown that the angular momentum of the current-carrying states can be transferred to the polarization state of the emitted photons [41]. Therefore, it is an intuitive method to obtain circularly polarized HHG that one increases the contributions of the selected current-carrying state, for example, the ionic state dominated by the selected current-carrying state [34,36]. However, there are still electrons with the opposite currents in the ion [34], which would decrease the intensity difference between high harmonics with opposite helicities. In fact, high harmonics from the two degenerate current-carrying states can be regarded as two HHG sources. Therefore, the interference between these HHG sources can make a contribution to the total HHG spectrum. If one can control the relative phase of the two HHG sources, one can expect the suppression of harmonic yields with the selected helicity, without needing to prepare the single current-carrying states. Degenerate current-carrying orbitals in polyatomic molecules may offer this possibility, where more degrees of freedom are involved.

In this work, we propose a scheme to obtain circularly polarized HHG and highly elliptically polarized attosecond pulses through the interference between HHG from degenerate highest occupied molecular orbitals (HOMOs). As a result of the interference, the large intensity differences between high harmonics with opposite helicities are achieved. However, for molecules with nondegenerate HOMO, their intensity is similar. This interference effect is related to noncylindrical symmetry of the molecular orbitals, so the intensity differences depend on the molecular orientation. Finally, we show that three-dimensional (3D) polyatomic molecules have more degrees of freedom for the control of HHG and demonstrate that ellipticity-tunable attosecond pulses can be obtained by controlling the molecular orientation.

II. THEORETICAL MODEL

HHG is investigated based on the molecular strong-field approximation (SFA) [42–44], which enables us to study the complex molecules with less computational consumptions. The time-dependent dipole moment is calculated with the integral

$$\mathbf{D}(t) = i\int_0^t dt' \left(\frac{\pi}{\epsilon + i\tau/2}\right)^{3/2} \mathbf{d}^*[\mathbf{p}_{st}(t,t') - \mathbf{A}(t)] \times \mathbf{E}(t') \cdot \mathbf{d}[\mathbf{p}_{st}(t,t') - \mathbf{A}(t')] e^{-iS_{st}(t,t')} + \text{c.c.} \quad (1)$$

$\mathbf{E}(t)$ is the electric field of the laser pulse. $\mathbf{A}(t)$ is the corresponding vector potential and ϵ is a small positive constant. $\mathbf{p}_{st}$ and S_{st} are the stationary momentum and quasiclassical action, which are given by

$$\mathbf{p}_{st}(t',t) = \frac{1}{t-t'}\int_{t'}^{t} \mathbf{A}(t'')dt'', \quad (2)$$

$$S_{st}(t,t') = \int_{t'}^{t} dt'' \left(\frac{[\mathbf{p}_{st} - \mathbf{A}(t'')]^2}{2} + I_p\right), \quad (3)$$

where I_p is the ionization potential of the molecule. The transition dipole moment between the ground state and the continuum state is calculated by

$$\mathbf{d}(\mathbf{p}) = \langle e^{-i\mathbf{p}\cdot\mathbf{r}} | \mathbf{r} | \psi_{\text{HOMO}} \rangle. \quad (4)$$

The HOMOs of molecules are obtained by using the Hartree-Fock method with the cc-pVTZ basis set as implemented in the GAUSSIAN09 program [45].

The radiation field in frequency domain can be obtained by the Fourier transform of the time-dependent dipole acceleration $\mathbf{a}(t)$:

$$\tilde{\mathbf{A}}(\Omega) \propto \int \mathbf{a}(t) e^{-i\Omega t} dt, \quad (5)$$

where $\mathbf{a}(t) = \ddot{\mathbf{D}}(t)$ and Ω is the frequency of the high harmonics. We also projected the radiation field on the right and left circular polarization vector, corresponding to $\hat{\mathbf{e}}_R = \frac{1}{\sqrt{2}}(\hat{\mathbf{e}}_x + i\hat{\mathbf{e}}_y)$ and $\hat{\mathbf{e}}_L = \frac{1}{\sqrt{2}}(\hat{\mathbf{e}}_x - i\hat{\mathbf{e}}_y)$, respectively. The right circular component $\tilde{A}_R(\Omega)$ and left circular component $\tilde{A}_L(\Omega)$ are given by $\tilde{A}_R(\Omega) = \frac{1}{\sqrt{2}}[\tilde{A}_x(\Omega) + i\tilde{A}_y(\Omega)]$ and $\tilde{A}_L(\Omega) = \frac{1}{\sqrt{2}}[\tilde{A}_x(\Omega) - i\tilde{A}_y(\Omega)]$, respectively. Finally, the intensity of right and left circular components of HHG can be calculated by

$$I_R(\Omega) = |\tilde{A}_R(\Omega)|^2, \quad I_L(\Omega) = |\tilde{A}_L(\Omega)|^2. \quad (6)$$

III. RESULTS AND DISCUSSIONS

A. HHG from the molecule with nondegenerate HOMO

As a comparison, we first present HHG from BCl_3 molecule induced by the BCCP fields. The HOMO of BCl_3 is nondegenerate and has no ring currents. As shown in Fig. 1(a), the geometry of this molecule is trigonal planar.

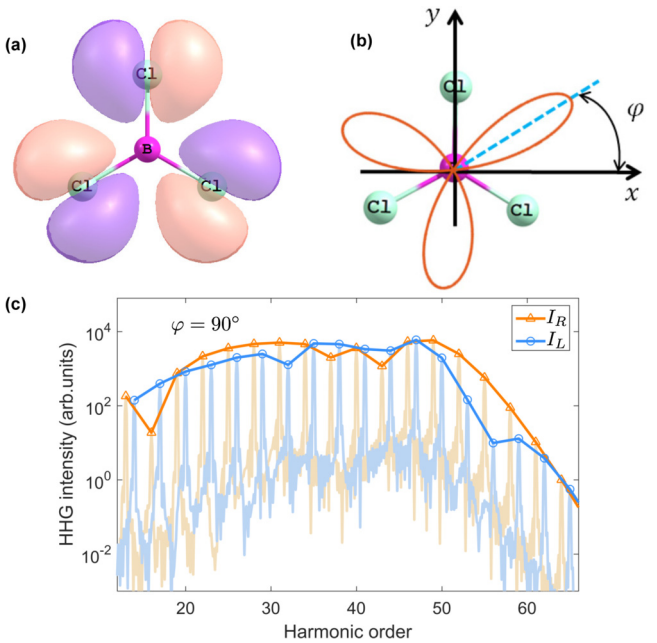

FIG. 1. (a) HOMO of BCl_3. (b) Sketch of the orientation angle φ between the molecular and the BCCP field. (c) HHG spectra projected onto left and right circular components for $\varphi = 90°$.

Both BCl_3 and its HOMO have C_3 symmetry. The BCCP field is defined by

$$\mathbf{E}(t) = \mathrm{Re}[E_1 f(t)\hat{\mathbf{e}}_R e^{-i\omega t} + E_2 f(t)\hat{\mathbf{e}}_L e^{-2i\omega t}]. \tag{7}$$

The x, y components of the BCCP field (7) are given by

$$\begin{aligned} E_x(t) &= E_1 f(t)\cos(\omega t) + E_2 f(t)\cos(2\omega t), \\ E_y(t) &= E_1 f(t)\sin(\omega t) - E_2 f(t)\sin(2\omega t). \end{aligned} \tag{8}$$

HHG should be dependent on the orientation between the molecules and the laser pulses because of noncylindrical symmetry of the molecular orbitals and the BCCP field. Here we only consider the case where the plane of BCl_3 is parallel to the polarization plane of the BCCP field [46]. We change the relative orientation between the BCCP field and the molecule by rotating the driving laser field. The laboratory frame is chosen such that the pulse propagates along the z axis and the B-Cl axis of BCl_3 is fixed along the y axis [see Fig. 1(b)]. We define φ as the rotation angle around z axis and Eq. (8) as the electric field of $\varphi = 0$. The electric field rotated by φ can be obtained as

$$\begin{bmatrix} E_x(\varphi,t) \\ E_y(\varphi,t) \end{bmatrix} = \begin{bmatrix} \cos\varphi & -\sin\varphi \\ \sin\varphi & \cos\varphi \end{bmatrix} \begin{bmatrix} E_x(t) \\ E_y(t) \end{bmatrix}. \tag{9}$$

We choose $E_1 = E_2 = 0.0377$ a.u. (corresponding to the total intensity of 2×10^{14} W/cm^2 for the BCCP field) and $\omega = 0.038$ (corresponding to 1200 nm).

HHG spectra with the BCCP laser field of $\varphi = 90^\circ$ are presented in Fig. 1(c). Both the BCCP field and BCl_3 possess threefold rotational symmetry [47], which only permits the emission of harmonics $3m+1$ and $3m+2$ ($m \in \mathbb{N}$). Furthermore, the neighboring harmonic orders $3m+1$ and $3m+2$ possess the opposite helicities [48,49]. The harmonics at order $3m+1$ are right circularly polarized and the harmonics at order $3m+2$ are left circularly polarized. As shown in Fig. 1(c), the intensities of right circularly polarized high harmonics (RCPHH) and left circularly polarized high harmonics (LCPHH) are comparable because the HOMO is not a current-carrying orbital. The small intensity differences between high harmonics with two opposite helicities result from the noncylindrical symmetry of BCl_3.

B. HHG from the molecule with doubly degenerate current-carrying HOMOs

Let us now consider the BH_3 molecules, which have the same C_3 symmetry as BCl_3. However, the Cl atoms are replaced by the H atoms in BH_3. The HOMO of BH_3 molecule is doubly degenerate. These two degenerate orbitals $|E_x\rangle$ and $|E_y\rangle$ are present in Fig. 2(a). Note that $|E_x\rangle$ and $|E_y\rangle$ do not have C_3 symmetry. On the other hand, we can resort to the spherical-basis representation of the two degenerate HOMOs by $|E_\pm\rangle = 1/\sqrt{2}(|E_x\rangle + i|E_y\rangle)$. In this configuration, an electron in $|E_+\rangle$ orbital circulates in the same sense as the right circularly polarized fields, while the $|E_-\rangle$ orbital is counterrotating. As shown in Fig. 2(b), the density distribution of $|E_+\rangle$ also has threefold rotation symmetry but the phase of $|E_+\rangle$ changes continuously from $-\pi$ to π. Contributed by two degenerate current-carrying orbitals, the total harmonic fields

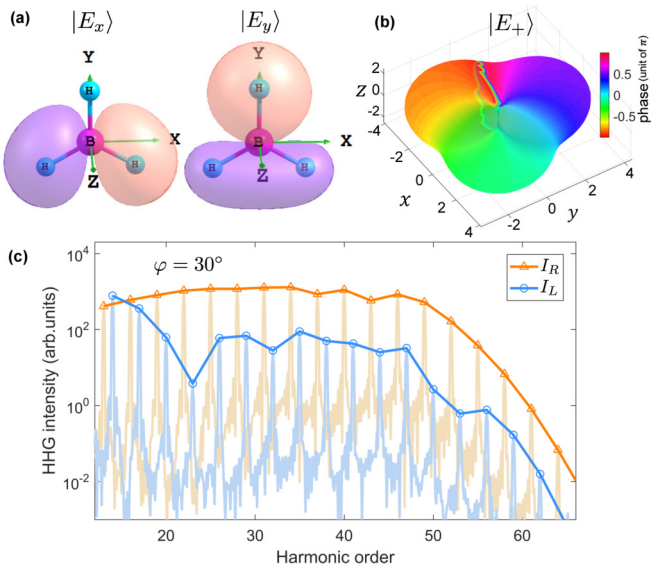

FIG. 2. (a) Two real degenerate HOMO $|E_x\rangle, |E_y\rangle$ of BH_3. (b) The ring-current HOMO $|E_+\rangle$ of BH_3. The color indicates the phase of $|E_+\rangle$. (c) HHG spectra projected onto left and right circular components for $\varphi = 30^\circ$.

$\tilde{A}(\Omega)$ from BH_3 can be obtained by

$$\tilde{A}(\Omega) = \tilde{A}^{(+)}(\Omega) + \tilde{A}^{(-)}(\Omega), \tag{10}$$

where $\tilde{A}^{(+)}(\Omega)$ and $\tilde{A}^{(-)}(\Omega)$ are the harmonic fields from $|E_+\rangle$ and $|E_-\rangle$ orbitals, respectively. From Fig. 2(c), one can see that HHG of BH_3 has the same selection rules as that of BCl_3. On the other hand, the RCPHH and LCPHH have different spectral shapes in the HHG spectrum of BH_3. Furthermore, one can see the distinct intensity differences between RCPHH and LCPHH, in contrast to that of BCl_3.

To evaluate the intensity differences between neighboring harmonics and obtain the energy-resolved ellipticity distribution, we define $\varepsilon_m = \frac{|\tilde{A}|_{3m+1} - |\tilde{A}|_{3m+2}}{|\tilde{A}|_{3m+1} + |\tilde{A}|_{3m+2}}$, where $|\tilde{A}|_{3m+1}$ and $|\tilde{A}|_{3m+2}$ are the amplitudes of harmonics $3m+1$ and $3m+2$, respectively. We calculate ε_m for different φ. As shown in Fig. 3, ε_m is dependent on the relative orientation angle φ due to the

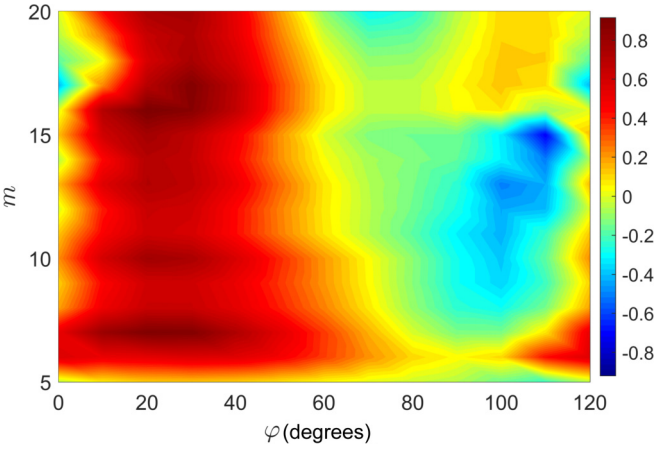

FIG. 3. ε_m of HHG from BH_3 as a function of φ and m.

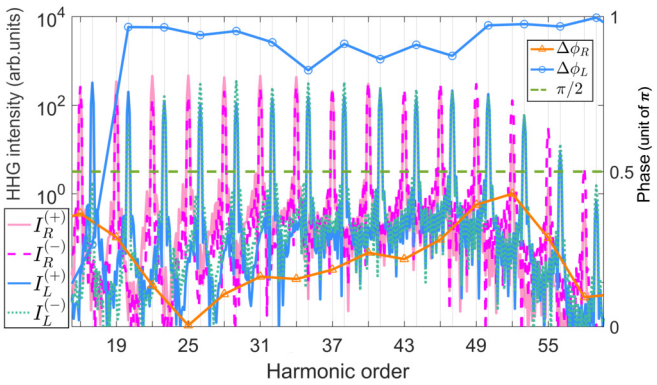

FIG. 4. Left axis: HHG intensities $I_R^{(+)}$, $I_R^{(-)}$, $I_L^{(+)}$, and $I_L^{(-)}$. Right axis: The phase difference between RCPHH (LCPHH) $\Delta\phi_R(\Delta\phi_L)$ from $|E_+\rangle$ and $|E_-\rangle$.

anisotropy of BH_3. On the other hand, ε_m is large in a wide range of φ.

C. Interference between HHG from degenerate current-carrying orbitals

To understand the intensity difference between RCPHH and LCPHH from BH_3. we need to separately study HHG from $|E_+\rangle$ and $|E_-\rangle$. For high harmonics with opposite helicities, we have expressions

$$\tilde{A}_R^{(+)}(\Omega) = \mathcal{A}_1(\Omega)e^{i\phi_1(\Omega)}, \quad \tilde{A}_L^{(+)}(\Omega) = \mathcal{A}_2(\Omega)e^{i\phi_2(\Omega)},$$
$$\tilde{A}_R^{(-)}(\Omega) = \mathcal{A}_3(\Omega)e^{i\phi_3(\Omega)}, \quad \tilde{A}_L^{(-)}(\Omega) = \mathcal{A}_4(\Omega)e^{i\phi_4(\Omega)}. \quad (11)$$

The upper right corner elements $(+)$ and $(-)$ in Eq. (11) represent the orbital $|E_+\rangle$ and $|E_-\rangle$ and the lower right corner elements R and L represent the helicities of high harmonics. According to Eq. (11), the intensities of RCPHH and LCPHH from $|E_+\rangle$ orbital are given by

$$I_R^{(+)} = |\tilde{A}_R^{(+)}|^2 = \mathcal{A}_1{}^2, \quad I_L^{(+)} = |\tilde{A}_L^{(+)}|^2 = \mathcal{A}_3{}^2. \quad (12)$$

Analogously, for $|E_-\rangle$ orbital, we have

$$I_R^{(-)} = |\tilde{A}_R^{(-)}|^2 = \mathcal{A}_2{}^2, \quad I_L^{(-)} = |\tilde{A}_L^{(-)}|^2 = \mathcal{A}_4{}^2. \quad (13)$$

The total intensity of RCPHH from these two orbitals can be obtained by

$$I_R = |\tilde{A}_R^{(+)} + \tilde{A}_R^{(-)}|^2 = I_R^{(+)} + I_R^{(-)} + 2\sqrt{I_R^{(+)}I_R^{(-)}}\cos\Delta\phi_R, \quad (14)$$

where $\Delta\phi_R = \phi_1 - \phi_3$. Analogously, we get

$$I_L = |\tilde{A}_L^{(+)} + \tilde{A}_L^{(-)}|^2 = I_L^{(+)} + I_L^{(-)} + 2\sqrt{I_L^{(+)}I_L^{(-)}}\cos\Delta\phi_L, \quad (15)$$

where $\Delta\phi_L = \phi_2 - \phi_4$.

The intensity and relative phase of HHG from $|E_+\rangle$ and $|E_-\rangle$ are presented in Fig. 4. One can see that $\Delta\phi_R$ (i.e., the relative phase between the RCPHH from these two states) is less than $\pi/2$, which leads to the constructive interference for RCPHH. For LCPHH, the phase difference $\Delta\phi_L$ is near π, which leads to the destructive interference. Meanwhile, the intensities of LCPHH from $|E_+\rangle$ and $|E_-\rangle$ are almost equal, which results in the strong destructive interference. Furthermore, this destructive interference occurs in a wide frequency range and therefore one can see the supression of LCPHH almost across the whole plateau. To summarize, the interference enhances the intensity of RCPHH and diminishes the intensity of LCPHH. So the HHG spectra of BH_3 display large intensity differences between LCPHH and RCPHH in broad bandwidth (see Fig. 3). However, there is no interference in HHG from BCl_3 because of nondegenerate HOMO. Therefore, for BCl_3, the intensities of RCPHH and LCPHH are comparable.

In fact, the interference effect may also be found in HHG from atoms with p orbitals [25]. However, for atoms, the relative intensity between $I_L^{(+)}$ and $I_L^{(-)}$ is always large due to the different recombination dipole moments and the spherical symmetry of the orbitals [25], which reduces the effect of the interference between LCPHH from p_+ and p_- orbitals (see the Appendixes). In polyatomic molecules, the strong destructive interference between LCPHH can be achieved with $I_L^{(+)} \approx I_L^{(-)}$ for a certain range of orientation angles (see Fig. 4).

Changing the intensity ratio of the BCCP field $I_\omega/I_{2\omega}$ results in the change of the electric field, which would consequently modify the interference between HHG from current-carry orbitals. When $I_\omega/I_{2\omega}$ is away from 1, i.e., the intensity ratio is too large or small, this driving laser field behaves more like a circularly polarized laser field. To explicitly show the transition of generated harmonics from the BCCP field to the circularly polarized laser field, we present HHG spectra with increasing $I_\omega/I_{2\omega}$ ratios in Appendix B. As shown in Fig. 10, the harmonic generation efficiency drops dramatically with an increasing $I_\omega/I_{2\omega}$ because of the decrease of the electron recombination probability. Therefore, one should consider the case of the intensity ratio $I_\omega/I_{2\omega} \approx 1$. Results in the range $I_\omega/I_{2\omega} \in [1/4, 4]$ are presented in Fig. 5. When I_ω and $I_{2\omega}$ are comparable, such as $I_\omega/I_{2\omega} = 3$ and $I_\omega/I_{2\omega} = 0.5$ [see Figs. 5(b) and 5(d)], ϵ_m has large positive value for a broad spectral range. To demonstrate the strong destructive interference for LCPHH, HHG spectrum with $I_\omega/I_{2\omega} = 3$ and $\varphi = 30^\circ$ is presented in Fig. 6(a). HHG from $|E_+\rangle$, $|E_-\rangle$, and the relative phase between high harmonics from these two orbitals are presented in Fig. 6(b). One can see that $I_L^{(+)} \approx I_L^{(-)}$ and $\Delta\phi_L \approx \pi$ in the frequency range from 26 to 59 orders, resulting in the strong destructive interference between LCPHH from $|E_+\rangle$ and $|E_-\rangle$. On the other hand, the phase difference $\Delta\phi_R$ is less than $\pi/2$, which leads to the constructive interference between the RCPHH from these two current-carrying orbitals. Therefore, the intensities of RCPHH are much higher than the intensity of LCPHH. When the intensity of the second harmonic $I_{2\omega}$ gets larger, such as $I_\omega/I_{2\omega} = 1/4$ [see Fig. 5(f)], the absolute values of ϵ_m get smaller resulting from the weak interference effect. According to our calculation results, for $I_\omega/I_{2\omega} = 1/4$, the intensity difference between $I_L^{(+)}$ and $I_L^{(-)}$ gets larger and the phase difference $\Delta\phi_L$ derives from π. Both of them lead to this weak interference effect.

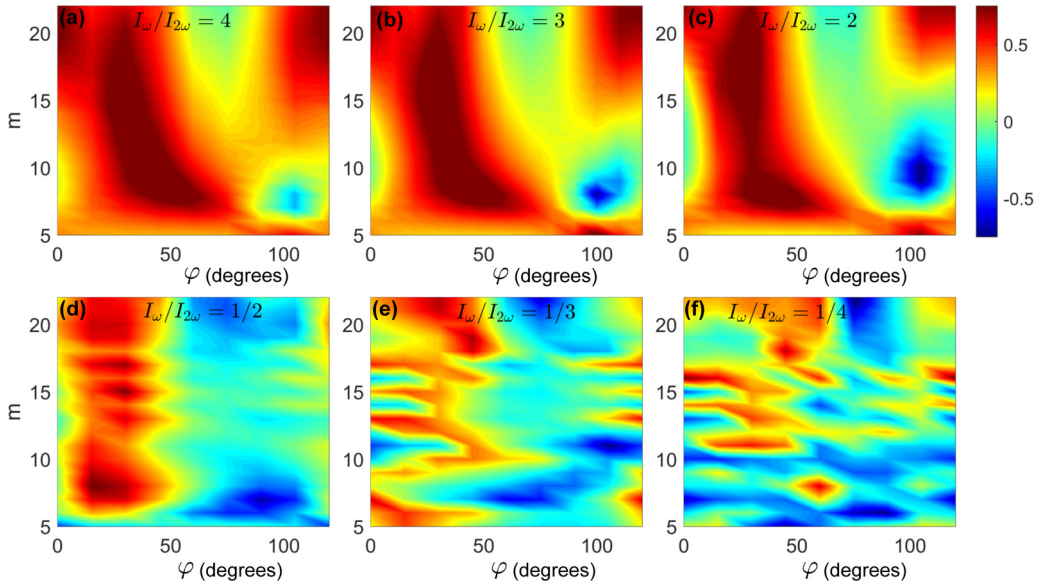

FIG. 5. ε_m with different intensity ratio $I_\omega/I_{2\omega}$.

D. HHG from the polar molecule with doubly degenerate current-carrying HOMOs

Now let us consider the polar molecules with degenerate current-carrying orbitals, for example, CH_3Cl. CH_3Cl molecule is obtained by replacing one of the H atoms in CH_4 with a Cl atom. Therefore, it also has C_3 symmetry. Meanwhile, it is a polar molecule which is convenient to accomplish orientation [50–52] and more degrees of freedom can be manipulated by their orientations. Similar to BH_3, CH_3Cl also have two real degenerate HOMO $|A_1\rangle$, $|A_2\rangle$ in the Cartesian basis. In spherical basis, its current-carrying HOMOs are $|A_\pm\rangle = (|A_1\rangle \pm i|A_2\rangle)/\sqrt{2}$. $|A_1\rangle$, $|A_2\rangle$ and one current-carrying orbital $|A_+\rangle$ are presented in Fig. 7(a). One can see that the orbitals localized on the methyl group are like the HOMOs of BH_3, while the orbitals localized on the Cl atom are like p orbitals of atoms. For the orientation of CH_3Cl, θ is defined as the angle between C-Cl axis and z axis [see Fig. 7(b)]. In addition, CH_3Cl have another degree of freedom, i.e., rotation around the C-Cl axis. So we defined β as the rotation angle of molecules around the C-Cl axis.

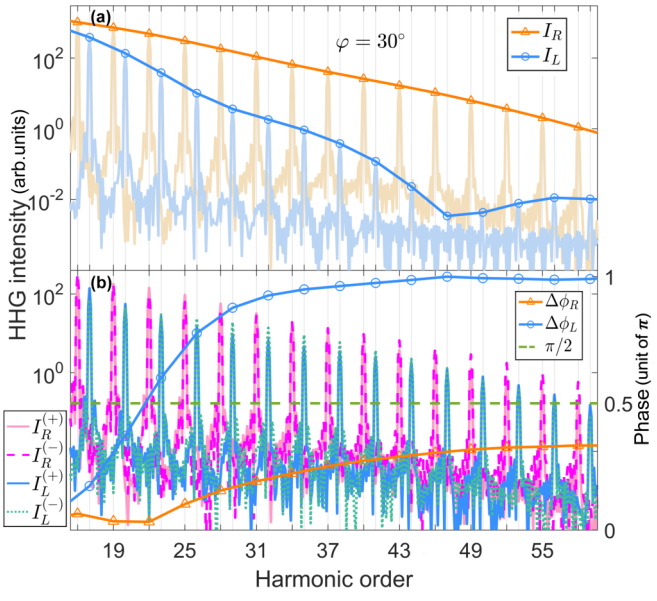

FIG. 6. (a) HHG spectra projected onto left and right circular components for $\varphi = 30°$ and $I_\omega/I_{2\omega} = 3$. (b) Left axis: HHG intensities $I_R^{(+)}$, $I_R^{(-)}$, $I_L^{(+)}$, and $I_L^{(-)}$. Right axis: The phase difference between RCPHH (LCPHH) $\Delta\phi_R$ ($\Delta\phi_L$) from $|E_+\rangle$ and $|E_-\rangle$.

HHG from CH_3Cl with $\theta = 0°$ and $\beta = 15°$ is present in Fig. 7(c). One can see, similar to BH_3, a strong suppression of LCPHH due to the interference effect, especially for 20th–35th. As shown in Fig. 7(d), ε_m is always positive for $\beta \in [0°, 40°]$ and $\beta \in [100°, 120°]$. When θ is changed, the Hamiltonian of the system does not have C_3 symmetry and the harmonics at $3m$ is permitted [see Fig. 7(e)]. There is still a ring current effect on the polarization plane of the laser field. So the interference between HHG from the two current-carrying orbitals still exits in the orientation of $\theta \neq 0°$. For example, the intensity differences still exit when $\theta = 30°$ [see Fig. 7(e)], which is caused by the interference. In addition, the polarization state of harmonics at $3m + 1$ and $3m + 2$ is not pure circular because of the breaking of the threefold symmetry. We calculated the ellipticity of HHG from CH_3Cl by $\epsilon = (|\tilde{A}_R| - |\tilde{A}_L|)/(|\tilde{A}_R| + |\tilde{A}_L|)$ when $\theta = 30°$. As shown in Fig. 7(f), harmonics in the range from 20th to 35th have large ellipticity for all β.

Finally, we will show the elliptically polarized attosecond pulses obtained by superposing the HHG from CH_3Cl molecules with different orientations. Since the C-Cl axis can be oriented while the molecules can be free to rotate around this axis, here we only consider one-dimensional orientation and phase matching is neglected; HHG for all β is added coherently to average the rotation around the C-Cl axis [53,54]. Figure 8(a) shows the electric vector of the attosecond pulse trains obtained by superposing 13th to 28th harmonics in the case of $\theta = 0°$. Three dominant bursts in one optical cycle are observed, which corresponds to the trefoil pattern of the driving field. We calculate the ratio of the minor axis and the major

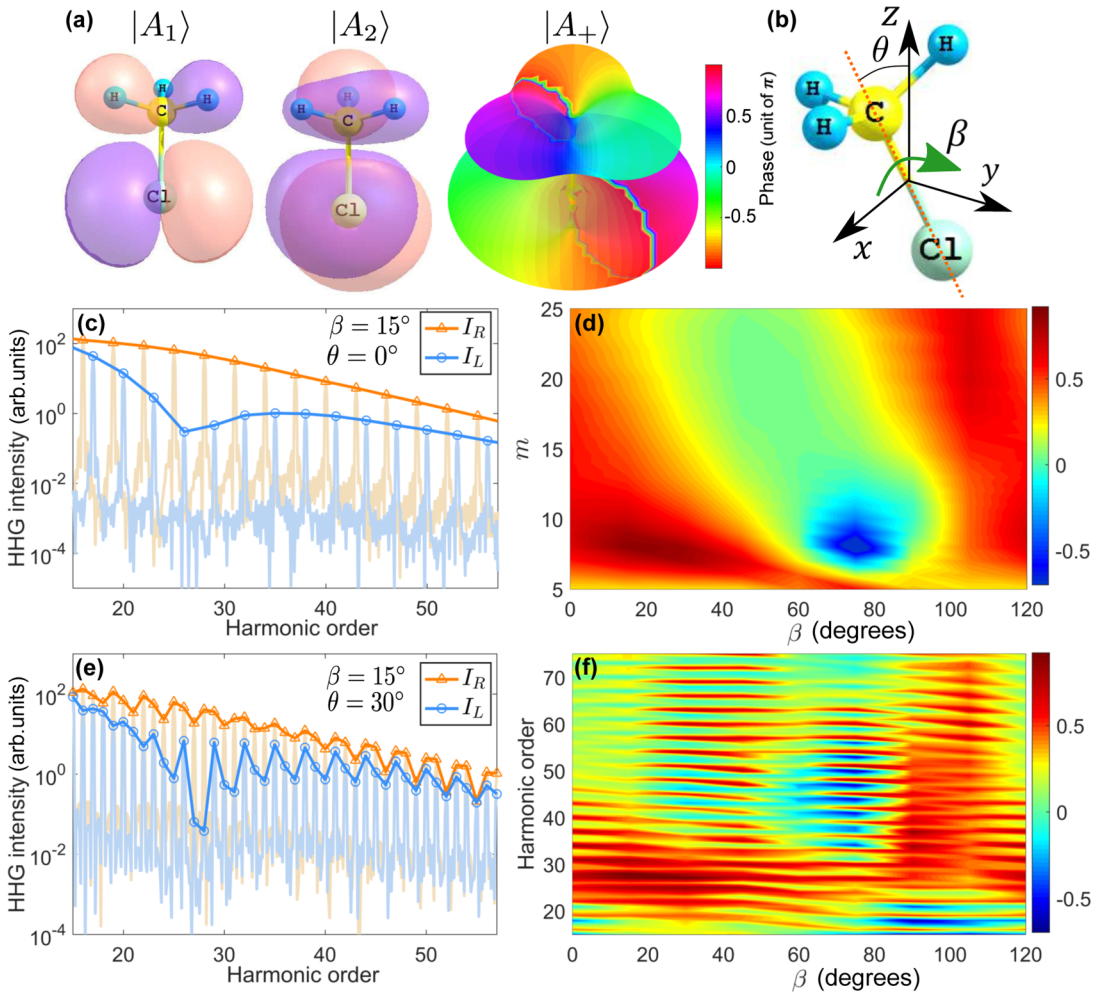

FIG. 7. (a) Two real degenerate HOMO ($|A_1\rangle$, $|A_2\rangle$) and one current-carrying orbital $|A_+\rangle$ of CH_3Cl. (b) Geometrical definitions: θ is defined as the angle between C-Cl axis and z axis. β is defined as the rotation angle of molecules around C-Cl axis. (c) HHG spectra projected onto left and right circular components when $\theta = 0°$ and $\beta = 15°$. (d) ε_m of HHG from CH_3Cl as a function of β and m. (e) HHG spectra projected onto left and right circular components when $\theta = 30°$ and $\beta = 15°$. (f) The ellipticity of HHG from CH_3Cl as a function of β and m.

axis of the elliptical polarized attosecond fields to evaluate the ellipticity of the pulses. As shown in Fig. 8(a), the ellipticity of the generated attosecond pulse is about 0.78 and the duration is 580 as. Note that the highly elliptically polarized attosecond pulses also can be obtained for BH_3. Figure 8(b) presents

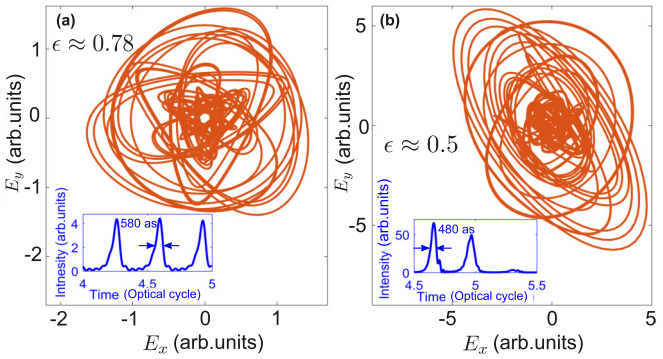

FIG. 8. Electric vector of the attosecond pulse obtained by superposing high harmonics when $\theta = 0°$ (a) and $\theta = 30°$ (b). The insets show the profiles of the attosecond pulses.

the attosecond pulse trains obtained by superposing 22th to 58th harmonics in the case of $\theta = 30°$. One can see that the ellipticity of the attosecond pulse is about 0.5 and the duration is about 480 as. Therefore, one can obtain highly elliptically polarized attosecond pulses with the interference between HHG from the degenerate current-carrying orbitals and the ellipticity of the pulses can be controlled by changing the molecular orientation.

Although we take two prototype molecules as examples in this work, the interference is independent of specific molecules and is a general phenomenon. The degenerate current-carrying state widely exists in atoms [25,34,35] and molecules with high symmetries [32,33]. Since the electrons occupied in degenerate current-carrying orbitals have opposite orbital angular momenta, they exhibit different responses to the (multicolor) circularly polarized driving fields and the radiation from them, as two light sources, interfere with each other. When the phase difference between high harmonics from these orbitals is near π, the destructive interference takes place. Furthermore, this destructive interference is strong when the intensities of high harmonics from these orbitals are comparable, which is available when the ring currents are

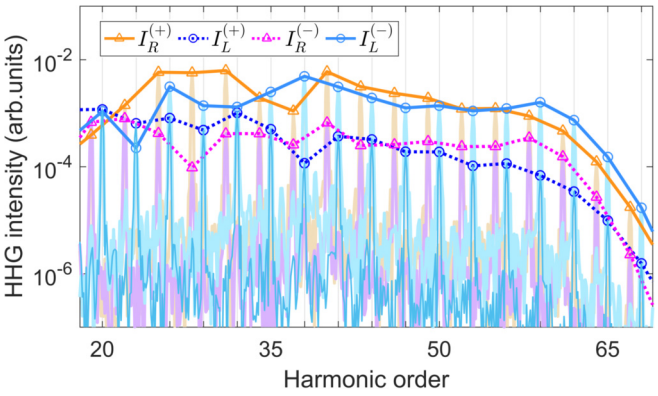

FIG. 9. (a) HHG intensities $I_R^{(+)}$, $I_R^{(-)}$, $I_L^{(+)}$, and $I_L^{(-)}$ of Ne atom. The laser parameters are the same as Fig. 4.

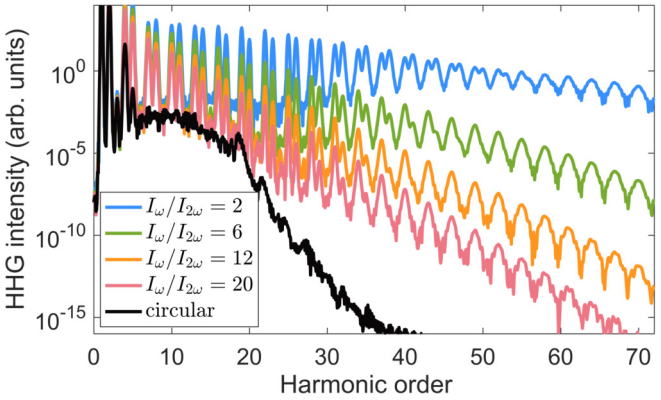

FIG. 10. HHG spectra with an increasing $I_\omega/I_{2\omega}$ of BCCP fields and the circularly polarized laser field.

no longer toroidal with optimized driving fields. Therefore, this dramatic destructive interference is found in polyatomic molecules rather than atoms.

IV. CONCLUSIONS

In summary, we study the interference between HHG from degenerate current-carrying orbitals of polyatomic molecules. Using this interference, one can obtain large intensity differences between high harmonics with opposite helicities in a broad spectral range. It is shown that the interference is destructive for the high harmonics with the selected helicity. The noncylindrical symmetry of the molecular current-carrying states plays an important role in the strong destructive interference for a certain range of molecular orientation. Furthermore, this interference effect can be controlled by adjusting the relative intensity ratio of the BCCP field. Finally, we demonstrate that, for polar molecules, more degrees of freedom than atoms are involved, which could also be used to tune the ellipticity of high harmonics. Although our scheme requires one more step, i.e., the orientation [50–52], than some methods with atomic noble gas, our method is favorable for applications when one needs highly elliptically polarized harmonics in a broad spectral range.

ACKNOWLEDGMENTS

This paper was supported by the National Natural Science Foundation of China under Grants No. 11774109, No. 11627809, No. 11574101, No. 11334009, No. 11425414, and No. 61475005.

APPENDIX A: HHG FROM ATOM WITH *p* ORBITALS

As we know, the amplitudes of recombination dipole moment, when the radiation has the same rotation with the ring current of the orbitals, is larger than that in the counter-rotating case. This is a direct analog of Fano-Bethe propensity rules [55] in atomic transitions that have been applied in the study of Rydberg atoms in microwave circular fields [56,57]. For atoms induced by the BCCP fields, the intensity of HHG is proportional to the recombination matrix element and therefore $I_L^{(-)}$ is much larger than $I_L^{(+)}$ [25,39]. This relation remains the same for all φ due to the spherical symmetry of the atom. So the condition for the destructive interference is not well fulfilled. Here we choose Ne atom as an example. To show the weaker interference effect in atoms, HHG spectra of single p_+ and p_- orbitals of the Ne atom induced by the BCCP field are presented in Fig. 9. One can see the large intensity differences between $I_L^{(-)}$ and $I_L^{(+)}$.

APPENDIX B: HHG SPECTRA WITH DIFFERENT $I_\omega/I_{2\omega}$

To show how the HHG spectra change from the BCCP fields to the circularly polarized laser field, we present HHG spectra with an increasing $I_\omega/I_{2\omega}$ and circularly polarized laser field in Fig. 10. In previous works, efficient high harmonics were found in the circularly polarized laser fields and it is demonstrated that these high harmonics originate mainly from the field-induced transitions between the bound states [58,59]. Therefore, these harmonics are usually limited in below-threshold ionization or the low-frequency region near the ionization threshold. In this work, we focus on harmonics with high photon energy where the transitions between the bound states have no contributions and HHG is dominated by the electron recombination process. Therefore, one cannot see the efficient harmonics with circularly polarized laser field even though they are symmetry allowed. HHG in the high photon energy region can be well described by our simulations based on SFA. Transitions between the bound states are not taken into account in SFA, which leads to the underestimate of the efficiency of below-threshold harmonics. However, this does not influence the discussions about the interference effect.

[1] F. Krausz and M. Ivanov, Rev. Mod. Phys. **81**, 163 (2009).
[2] M. Hentschel, R. Kienberger, C. Spielmann, G. A. Reider, N. Milošević, T. Brabec, P. Corkum, U. Heinzmann, M. Drescher, and F. Krausz, Nature (London) **414**, 509 (2001).
[3] J. Li, X. Ren, Y. Yin, K. Zhao, A. Chew, Y. Cheng, E. Cunningham, Y. Wang, S. Hu, Y. Wu, M. Chini, and Z. Chang, Nat. Commun. **8**, 186 (2017).

[4] T. Gaumnitz, A. Jain, Y. Pertot, M. Huppert, I. Jordan, F. Ardana-Lamas, and H. J. Worner, Opt. Express **25**, 27506 (2017).

[5] L. Plaja, R. Torres, and A. Zaïr, *Attosecond Physics: Attosecond Measurements and Control of Physical Systems*, Springer Series in Optical Sciences Vol. 177 (Springer, New York, 2013).

[6] B. Wang, L. He, Y. He, Y. Zhang, R. Shao, P. Lan, and P. Lu, Opt. Express **27**, 30172 (2019); Z. Yang, W. Cao, X. Chen, J. Zhang, Y. Mo, H. Xu, K. Mi, Q. Zhang, P. Lan, and P. Lu, Opt. Lett. **45**, 567 (2020); K. Mi, W. Cao, H. Xu, Y. Mo, Z. Yang, P. Lan, Q. Zhang, and P. Lu, Phys. Rev. Appl. **13**, 014032 (2020).

[7] P. B. Corkum, Phys. Rev. Lett. **71**, 1994 (1993).

[8] V. V. Strelkov, A. A. Gonoskov, I. A. Gonoskov, and M. Y. Ryabikin, Phys. Rev. Lett. **107**, 043902 (2011); Y. Zhao, Y. Zhou, J. Liang, Z. Zeng, Q. Ke, Y. Liu, M. Li, and P. Lu, Opt. Express **27**, 21689 (2019).

[9] A. Ferré, C. Handschin, M. Dumergue, F. Burgy, A. Comby, D. Descamps, B. Fabre, G. A. Garcia, R. Géneaux, L. Merceron, E. Mével, L. Nahon, S. Petit, B. Pons, D. Staedter, S. Weber, T. Ruchon, V. Blanchet, and Y. Mairesse, Nat. Photon. **9**, 93 (2015).

[10] O. Travnikova, J.-C. Liu, A. Lindblad, C. Nicolas, J. Söderström, V. Kimberg, F. Gel'mukhanov, and C. Miron, Phys. Rev. Lett. **105**, 233001 (2010).

[11] D. D. Hickstein, F. J. Dollar, P. Grychtol, J. L. Ellis, R. Knut, C. Hernández-García, D. Zusin, C. Gentry, J. M. Shaw, T. Fan, K. M. Dorney, A. Becker, A. Jaroń-Becker, H. C. Kapteyn, M. M. Murnane, and C. G. Durfee, Nat. Photon. **9**, 743 (2015).

[12] O. Kfir, P. Grychtol, E. Turgut, R. Knut, D. Zusin, D. Popmintchev, T. Popmintchev, H. Nembach, J. M. Shaw, A. Fleischer, H. Kapteyn, M. Murnane, and O. Cohen, Nat. Photon. **9**, 99 (2015).

[13] T. Fan, P. Grychtol, R. Knut, C. Hernández-García, D. D. Hickstein, D. Zusin, C. Gentry, F. J. Dollar, C. A. Mancuso, C. W. Hogle, O. Kfir, D. Legut, K. Carva, J. L. Ellis, K. M. Dorney, C. Chen, O. G. Shpyrko, E. E. Fullerton, O. Cohen, P. M. Oppeneer, D. B. Milošević, A. Becker, A. A. Jaroń-Becker, T. Popmintchev, M. M. Murnane, and H. C. Kapteyn, Proc. Natl. Acad. Sci. USA **112**, 14206 (2015).

[14] S.-Y. Xu, M. Neupane, C. Liu, D. Zhang, A. Richardella, L. Andrew Wray, N. Alidoust, M. Leandersson, T. Balasubramanian, J. Sánchez-Barriga, O. Rader, G. Landolt, B. Slomski, J. Hugo Dil, J. Osterwalder, T.-R. Chang, H.-T. Jeng, H. Lin, A. Bansil, N. Samarth, and M. Zahid Hasan, Nat. Phys. **8**, 616 (2012).

[15] Y. Liu, G. Bian, T. Miller, and T. C. Chiang, Phys. Rev. Lett. **107**, 166803 (2011).

[16] X. Zhou, R. Lock, N. Wagner, W. Li, H. C. Kapteyn, and M. M. Murnane, Phys. Rev. Lett. **102**, 073902 (2009).

[17] Y. Mairesse, J. Higuet, N. Dudovich, D. Shafir, B. Fabre, E. Mevel, E. Constant, S. Patchkovskii, Z. Walters, M. Y. Ivanov, and O. Smirnova, Phys. Rev. Lett. **104**, 213601 (2010).

[18] A. Etches, C. B. Madsen, and L. B. Madsen, Phys. Rev. A **81**, 013409 (2010).

[19] A. Fleischer, O. Kfir, T. Diskin, P. Sidorenko, and O. Cohen, Nat. Photon. **8**, 543 (2014).

[20] K. M. Dorney, J. L. Ellis, C. Hernández-García, D. D. Hickstein, C. A. Mancuso, N. Brooks, T. Fan, G. Fan, D. Zusin, C. Gentry, P. Grychtol, H. C. Kapteyn, and M. M. Murnane, Phys. Rev. Lett. **119**, 063201 (2017).

[21] A. D. Bandrauk, J. Guo, and K. J. Yuan, J. Opt. **19**, 124016 (2017).

[22] S. Odžak and D. B. Milošević, Phys. Rev. A **92**, 053416 (2015).

[23] D. M. Reich and L. B. Madsen, Phys. Rev. A **93**, 043411 (2016).

[24] D. B. Milošević, W. Becker, and R. Kopold, Phys. Rev. A **61**, 063403 (2000).

[25] D. Baykusheva, S. Brennecke, M. Lein, and H. J. Wörner, Phys. Rev. Lett. **119**, 203201 (2017); D. Baykusheva, M. S. Ahsan, N. Lin, and H. J. Wörner, *ibid.* **116**, 123001 (2016).

[26] P.-C. Huang, C. Hernández-García, J.-T. Huang, P.-Y. Huang, C.-H. Lu, L. Rego, D. D. Hickstein, J. L. Ellis, A. Jaron-Becker, A. Becker, S.-D. Yang, C. G. Durfee, L. Plaja, H. C. Kapteyn, M. M. Murnane, A. H. Kung, and M.-C. Chen, Nat. Photon. **12**, 349 (2018).

[27] C. Hernández-García, C. G. Durfee, D. D. Hickstein, T. Popmintchev, A. Meier, M. M. Murnane, H. C. Kapteyn, I. J. Sola, A. Jaron-Becker, and A. Becker, Phys. Rev. A **93**, 043855 (2016).

[28] J. L. Ellis, K. M. Dorney, C. G. Durfee, C. Hernández-García, F. Dollar, C. A. Mancuso, T. Fan, D. Zusin, C. Gentry, P. Grychtol, H. C. Kapteyn, M. M. Murnane, and D. D. Hickstein, Opt. Express **25**, 10126 (2017).

[29] N. Tancogne-Dejean, O. D. Mucke, F. X. Kartner, and A. Rubio, Nat. Commun. **8**, 745 (2017).

[30] Z. Y. Chen and R. Qin, Opt. Express **27**, 3761 (2019); L. Li, P. Lan, L. He, W. Cao, Q. Zhang, and P. Lu, arXiv:1908.07283 [physics.optics].

[31] L. Li, P. Lan, X. Zhu, T. Huang, Q. Zhang, M. Lein, and P. Lu, Phys. Rev. Lett. **122**, 193901 (2019); J. Li, Q. Zhang, L. Li, X. Zhu, T. Huang, P. Lan, and P. Lu, Phys. Rev. A **99**, 033421 (2019).

[32] K. Liu, K. Renziehausen, and I. Barth, Phys. Rev. A **95**, 063410 (2017).

[33] I. Barth, J. Manz, Y. Shigeta, and K. Yagi, J. Am. Chem. Soc. **128**, 7043 (2006).

[34] S. Eckart, M. Kunitski, M. Richter, A. Hartung, J. Rist, F. Trinter, K. Fehre, N. Schlott, K. Henrichs, L. P. H. Schmidt, T. Jahnke, M. Schöffler, K. Liu, I. Barth, J. Kaushal, F. Morales, M. Ivanov, O. Smirnova, and R. Dörner, Nat. Phys. **14**, 701 (2018).

[35] G. S. J. Armstrong, D. D. A. Clarke, A. C. Brown, and H. W. van der Hart, Phys. Rev. A **99**, 023429 (2019).

[36] A. Hartung, F. Morales, M. Kunitski, K. Henrichs, A. Laucke, M. Richter, T. Jahnke, A. Kalinin, M. Schöffler, L. P. H. Schmidt, M. Ivanov, O. Smirnova, and R. Dörner, Nat. Photon. **10**, 526 (2016).

[37] T. Herath, L. Yan, S. K. Lee, and W. Li, Phys. Rev. Lett. **109**, 043004 (2012).

[38] I. Barth and O. Smirnova, Phys. Rev. A **84**, 063415 (2011).

[39] L. Medišauskas, J. Wragg, H. van der Hart, and M. Y. Ivanov, Phys. Rev. Lett. **115**, 153001 (2015); X. Zhu, P. Lan, K. Liu, Y. Li, X. Liu, Q. Zhang, I. Barth, and P. Lu, Opt. Express **24**, 4196 (2016).

[40] O. Neufeld and O. Cohen, Phys. Rev. Lett. **123**, 103202 (2019).

[41] X. Xie, A. Scrinzi, M. Wickenhauser, A. Baltuska, I. Barth, and M. Kitzler, Phys. Rev. Lett. **101**, 033901 (2008); X. Zhang, L. Li, X. Zhu, K. Liu, X. Liu, D. Wang, P. Lan, I. Barth, and P. Lu, Phys. Rev. A **98**, 023418 (2018).

[42] X. X. Zhou, X. M. Tong, Z. X. Zhao, and C. D. Lin, Phys. Rev. A **72**, 033412 (2005); S. Luo, M. Li, W. Xie, K. Liu, Y. Feng, B. Du, Y. Zhou, and P. Lu, *ibid.* **99**, 053422 (2019); J. Tan, Y. Zhou, Q. Ke, M. He, J. Liang, Y. Li, M. Li, and P. Lu, *ibid.* **101**, 013407 (2020).
[43] D. B. Milošević, J. Mod. Opt. **66**, 47 (2018).
[44] I. Petersen, J. Henkel, and M. Lein, Phys. Rev. Lett. **114**, 103004 (2015).
[45] M. J. Frisch *et al.*, *Gaussian09, Revision A.02*, Gaussian, Inc., Wallingford, CT, 2016.
[46] J. Maurer, D. Dimitrovski, L. Christensen, L. B. Madsen, and H. Stapelfeldt, Phys. Rev. Lett. **109**, 123001 (2012).
[47] K. J. Yuan and A. D. Bandrauk, Phys. Rev. A **97**, 023408 (2018).
[48] X. Liu, X. Zhu, L. Li, Y. Li, Q. Zhang, P. Lan, and P. Lu, Phys. Rev. A **94**, 033410 (2016).
[49] O. Neufeld, D. Podolsky, and O. Cohen, Nat. Commun. **10**, 405 (2019).
[50] L. Holmegaard, J. L. Hansen, L. Kalhøj, S. Louise Kragh, H. Stapelfeldt, F. Filsinger, J. Küpper, G. Meijer, D. Dimitrovski, M. Abu-samha, C. P. J. Martiny, and L. Bojer Madsen, Nat. Phys. **6**, 428 (2010).
[51] S. Trippel, T. Mullins, N. L. M. Muller, J. S. Kienitz, R. Gonzalez-Ferez, and J. Kupper, Phys. Rev. Lett. **114**, 103003 (2015).
[52] S. Trippel, T. G. Mullins, N. L. M. Müller, J. S. Kienitz, K. Długołęcki, and J. Küpper, Mol. Phys. **111**, 1738 (2013).
[53] M. Lein, Phys. Rev. Lett. **94**, 053004 (2005).
[54] M. Lein, R. De Nalda, E. Heesel, N. Hay, E. Springate, R. Velotta, M. Castillejo, P. L. Knight, and J. P. Marangos, J. Mod. Opt. **52**, 465 (2005).
[55] U. Fano, Phys. Rev. A **32**, 617 (1985).
[56] K. Rzazewski and B. Piraux, Phys. Rev. A **47**, R1612(R) (1993).
[57] J. Zakrzewski, D. Delande, J. C. Gay, and K. Rzazewski, Phys. Rev. A **47**, R2468 (1993).
[58] V. Averbukh, O. E. Alon, and N. Moiseyev, Phys. Rev. A **64**, 033411 (2001).
[59] P. Žďánská, V. Averbukh, and N. Moiseyev, J. Chem. Phys. **118**, 8726 (2003).